KSME

Springer

Journal of Mechanical Science and Technology 36 (9) 2022

Original Article
DOI 10.1007/s12206-022-0828-9

Keywords:
· Comsol software
· In-situ preheating
· Temperature field
· Temperature gradient

Correspondence to:
Fangping Yao
yyaofangping@163.com

Citation:
Yin, H., LI, J., Zhao, L., Yao, F. (2022). Simulation of in-situ preheating of ni-based multi-layer and multi-pass coatings on H13 steel. Journal of Mechanical Science and Technology 36 (9) (2022) 4671~4680.
http://doi.org/10.1007/s12206-022-0828-9

Received October 18th, 2021
Revised April 12th, 2022
Accepted May 19th, 2022

† Recommended by Editor
Ja Choon Koo

Simulation of in-situ preheating of ni-based multi-layer and multi-pass coatings on H13 steel

Honggang Yin[1], Jinhua LI[1], Liwei Zhao[2] and Fangping Yao[1]

[1]Department of Mechanical Engineering and Automation, Liaoning University of Technology, Jinzhou 121001, China, [2]Nuoxintianpeng Limited Company of Technology, Tianjin 301700, China

Abstract COMSOL was used to simulate the temperature field of the preheating and non-preheating processes of the laser cladding multi-layer and multi-pass coating, and experimental verification was carried out. The results show that the temperature gradient value of the coating at the Z-axis is much larger than the value at the X and Y-axis, respectively. It indicates that the coating is sensitive to cracks at the Z-axis. After preheating, the quality of the coating is improved, and the results of the geometric morphology in experiments are basically consistent with the results of simulation. With increase in coating temperature, the cladding efficiency increased. The difference of temperature between the first and second layer was significantly reduced. The temperature gradient value at the Z-axis decreased. The coating grain structure presents as refined and well-distributed. The temperature gradient size in each layer decreased with the number of coatings increasing.

1. Introduction

In-situ preheating is performed by directly scanning the substrate placed on the laser table at a lower laser power [1]. This method is suitable for the preheating of thin small experimental substrates and large gear molds. The traditional preheating method is used to preheat the substrate before laser cladding by using a heating furnace and other methods, and then using a tool to place it on the laser table for laser cladding. This cumbersome process poses a safety hazard to the staff. Compared with a traditional preheating method, in-situ preheating has the characteristics of safety and reliability, short working cycle and low cost. Therefore, studying the effects of in-situ preheating on the morphology of multi-layer and multi-pass cladding layers is of great significance to the repaired technology development of gear mold in the future.

Establishing a laser cladding simulation model was an important tool to explore the morphology and temperature changes of multi-layer and multi-pass cladding layers, which has gradually attracted attention from many scholars in recent years. Fang et al. [2] showed that five kinds of materials were treated by multi-layer and multi-pass laser cladding with preheating and non-preheating, and the physical characteristic data was obtained from the experiments. A finite element model including phase transition was developed to study the effects of temperature on the residual stress of multi-layer and multi-pass laser cladding. Simon et al. [3] explored that the influence of process parameters on the morphology of the molten pool was studied based on a two-dimensional finite element model in COMSOL, which the molten pool was described by using mass, momentum, energy conservation equations and "moving grids". Li et al. [4] published that the temperature field of laser cladding for powder Stellite6 cobalt-based on the substrate surface of H13 steel was simulated by using the finite element method. The influence of different process parameters on the temperature field of a single laser cladding was analyzed, the best process parameter was calculated, the temperature field distribution of multi-pass laps were simulated, and the temperature gradient and the cooling rate at the edge of the molten pool were obtained. Sun et al. [5] established a three-dimensional finite element model

of multilayer laser cladding based on ANSYS "life and death unit" technology, and obtained the distribution law of the temperature field of multi-layer laser cladding. Meanwhile, the influence of preheating temperature on the thermal cycle of laser cladding was analyzed. Sun [6] established a synchronous powder feeding laser multi-pass cladding model based on ANSYS "life and death unit" technology, simulated the cladding of Ni60 alloy powder on the surface of 45 steel, and obtained the steady-state temperature field in laser cladding process. The influence of substrate preheating on the cladding layer was also analyzed.

Although researchers have carried out many studies related to finite element simulation of laser cladding, which have strong reference value, there are still some gaps in research on the preheating and non-preheating temperature fields and temperature gradients of multi-layer and multi-pass coatings.

Laser heat source models are generally divided into three models: Point heat source, Gaussian surface heat source, and double ellipsoid heat source. Compared with the other two models, the Gaussian surface heat source model can better reflect the decay law of the laser heat source, and can describe the process parameters that need to be controlled in the laser cladding process. Meanwhile, COMSOL is a simulation software with high openness, easy operation, superior computing performance, powerful post-processing capability and good at solving multi-physics coupling problems. Thus, based on the Gaussian heat source model, this paper aims to (a) simulate the process of in-situ preheating of H13 steel and the dynamic laser cladding process of multi-layer and multi-pass cladding layers by COMSOL, (b) draw the temperature-time change curves and the temperature gradients change curves, (c) analyze the influence of in-situ preheating on the morphology of multi-layer and multi-pass cladding layers, and (d) perform the experimental verification.

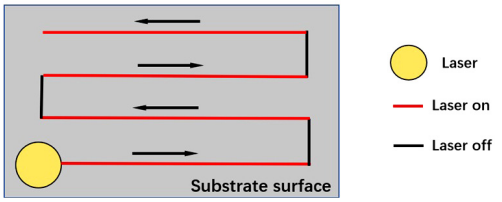

Fig. 1. Schematic diagram of preheating process.

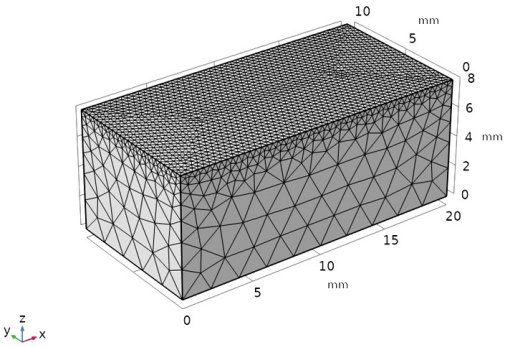

Fig. 2. Finite element meshing.

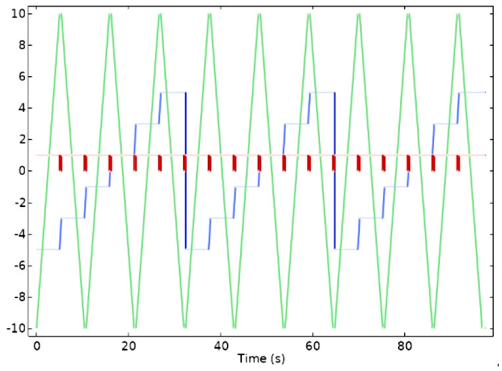

Fig. 3. Moving path of laser center and laser switch.

2. Preheat and non-preheat simulation

2.1 Warm-up simulation

2.1.1 Establishment of finite element model of laser preheating

It is necessary to design the path of the laser preheating before the preheating process of the substrate [7]. As shown in Fig. 1, a reciprocating path is adopted in this study, the time interval of scanning between each layer is set as 5 s, and the substrate is scanned three times to preheat. The area is scanned with 20 mm×10 mm, and the distance between adjacent passes is set as 1.5 mm. The energy distribution of the laser spots is simplified to a circular pie, that is, the energy is evenly distributed in the circle, and the outside of the circle has no energy. The laser power is 500 W, and the radius of laser spot is 1.5 mm. The substrate is H13 steel [8], the material of the cladding layer is Ni60 alloy powder, and the size of the substrate is set as 20 mm×10 mm×8 mm. COMSOL is applied for simulation. During the laser cladding process, the temperature of the upper surface of the substrate changes very drastically. Therefore, to accurately analyze the temperature change law of the cladding layer, it is necessary to refine the grid in this area. Furthermore, the area farther from the cladding layer is appropriately roughened to improve the efficiency. Meshing is performed in COMSOL, as shown in Fig. 2.

In laser cladding, reasonable planning of the scanning path is very important to the cladding quality of the multilayer and multi-pass cladding layers. As shown in Fig. 3, at 0-5 s, the laser scans along the X-axis, and the coordinates of the laser center (x_1, y_1) only change the value of x_1. At this time, the laser has remained on (f(x) = 1). At 5-5.4 s, the laser has been turned off (f(x) = 0).

And the center of the circle corresponding to the laser head moved along the Y axis. At this point, the x_1 value of the center of the circle stops changing and the y_1 value starts to change. Eq. (1) is used for the expression of energy distribution, which is absorbed by the laser on the surface of the substrate at the

position (x, y) as follows:

$$Q(x,y) = \frac{sign(sign(r^2 - (x - x_1)^2 - (y - y_1)^2) + 1)\eta P}{\pi r^2} \quad (1)$$

where P is the laser power, r is the laser spot radius, Q is the heat flow at the position (x, y) at a certain moment, η is the effective absorption rate of the substrate surface, and the position of the laser circle center is (x_1, y_1).

The area where the laser acts is changed after the position of the center of the circle (x_1, y_1) changing. Eq. (2) is used for the expression of laser displacement as follows:

$$x_1 = x\_f(t), y_1 = y\_f(t) \quad (2)$$

where laser_f(t) is represented to the on-off state of the laser (1 represents on, 0 represents off), and x_f(t) and y_f(t) are represented to the relationship between the position of laser center and time in COMSOL.

2.1.2 Analysis of temperature field during preheating

Based on the finite element model, the simulation in the process of laser preheating [9] is carried out by using the solution module of COMSOL simulation. Figs. 4(a)-(d) show the results of the surface temperature field distribution of the substrate at 13 s, 40 s, 57 s and 89 s, respectively. In 13 s, the lowest temperature of the substrate has increased from 293.15 K to 330 K, and the highest temperature on the upper surface of the substrate was 649 K. In 89 s, the lowest and the highest temperature of the upper surface increases to 460 K and 763 K, respectively.

2.2 Simulation of temperature field of preheated and non-preheated dynamic cladding layer

2.2.1 Establishment of finite element model of laser cladding process

At present, there are many studies on the morphology and temperature field simulation of the cladding layer using the "life and death unit" method. Due to the use of preset grids to simulate the increase in the volume of the cladding layer, the simulation results are quite different from the experimental results. Thus, in this paper, a deformed grid is used to realize the simulation of the dynamic cladding layer.

As shown in Fig. 6, a layer of Ni60 alloy powder is pre-laid on the upper surface of the substrate. While considering the mesh refinement in this area, in order to improve the scalability of the deformed mesh, a boundary layer mesh is set on the upper surface. Meshing is performed in COMSOL, as shown in Fig. 5.

In this paper, the movement of the laser cladding and the opening and closing of the laser are controlled by using piecewise functions. As shown in Fig. 7, when scanning along the X-axis, the laser is turned on for the laser cladding process.

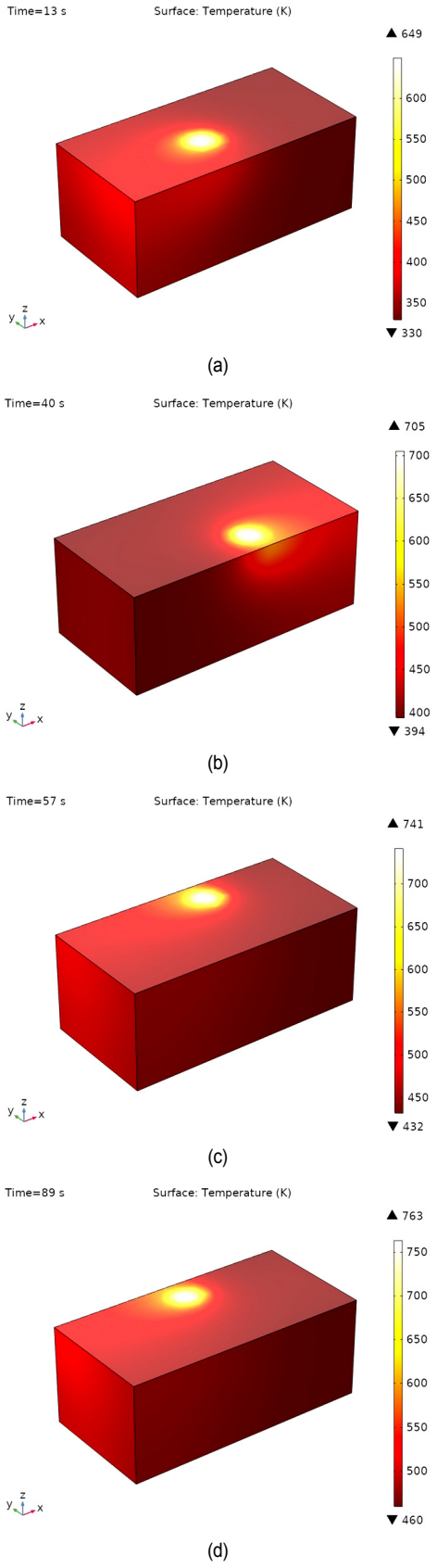

Fig. 4. Temperature field distribution of sample surface at several different time nodes after laser preheating: (a) 13 s; (b) 40 s; (c) 57 s; (d) 89 s.

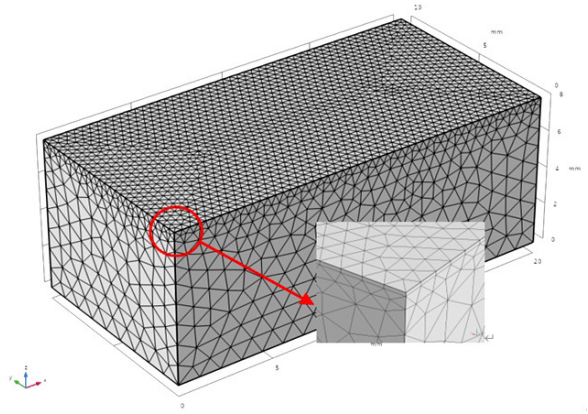

Fig. 5. Finite element meshing.

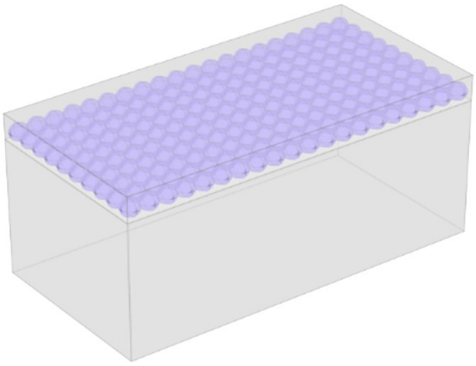

Fig. 6. Microscopic powder spreading model of metal powder.

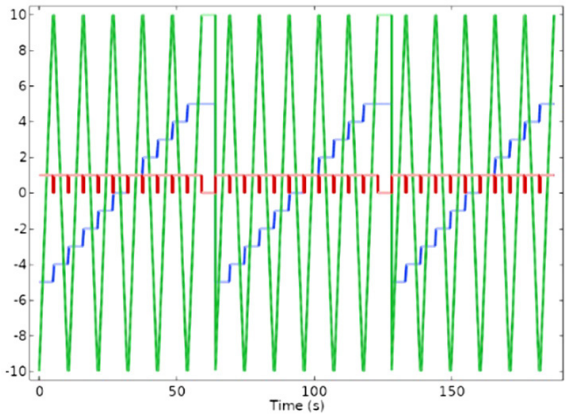

Fig. 7. Moving path of laser center and laser switch.

When scanning along the Y-axis, the laser is turned off. The first layer of laser cladding is completed in 59 s, the next layer of laser cladding is started after the laser being turned off for 5 s, and the second and third layers of laser cladding are completed in 123 s and 187 s, respectively.

It is assumed that the powder is uniformly distributed within the powder feeding radius R_1. Eq. (3) is used to the expression of powder feeding amount per unit area at coordinates (x, y) as follows:

$$M_{ba} = \frac{sign(sign(R_1^2 - (x - x_1)^2 - (y - y_1)^2) + 1)s}{\pi R_1^2} \tag{3}$$

where S represents the powder feeding rate, (x_1, y_1) is the powder feeding center, and the powder feeding center coincides with the laser circle center, which is the coaxial powder feeding. The position within the powder feeding radius R_1 is supplied with powder, and the other positions are not supplied. During the laser cladding process, the height of the substrate gradually increases with the time change, Eqs. (4)-(7) is used to the expression of the speed at which the height of the substrate increases as follows:

$$V_o = V_h D \tag{4}$$

$$V_h = V_{max} D_1 \tag{5}$$

$$D_1 = min\left(\frac{Q_{xy} D_p}{C(T - T_m)M_{ba}}, 1\right) \tag{6}$$

$$D = 1 - sign(sign(z - z_1 - z_2) + 1)D_{r1} + sign(sign(z_1 - z - z_2) + 1)D_{r2} \tag{7}$$

where V_h represents the speed at which the height of the substrate increased, V_{max} represents the maximum speed at which the height of the substrate increased, D_1 refers to the coefficient of cladding efficiency under laser irradiation, D_p represents the proportion of laser energy is absorbed by the metal powder here, C is the specific heat capacity of the powder, T refers to the surface temperature, T_m refers to the initial room temperature of the powder. D represents the coefficient of the shape factor, z represents the height of the place, z_1 represents the average height of the melting area and z_2 represents a reasonable height difference. D_{r1} and D_{r2} are positive numbers less than 1, which can be adjusted according to the experimental results.

The substrate and cladding material are H13 steel and Ni60 alloy powder, respectively. The chemical composition of the substrate and powder is shown in Table 1. According to the chemical composition of the substrate and powder, the corresponding material is selected through the material library in COMSOL.

2.2.2 Simulation parameters and sample point positions

The main parameters of laser cladding laser power are 1500 W, scanning speed is 4 mm/s, laser radius is 1.5 mm, powder feeding rate is 15 g/min, track spacing is 1 mm and effective absorption rate on the substrate surface is 12 %. The position of 16 points in the cladding layer is selected to add the probe, and the temperature change data is recorded timely as shown in Fig. 8. To ensure the representativeness and accuracy of the sample points and the reduction of the experimental error, a cross section is selected in the middle position where the cladding is relatively stable.

Table 1. Chemical compositions of H13 steel and Ni60.

Element	C	Si	Mn	Cr	Mo	V	P	S	Fe	B	Ni
H13 (%)	0.38	0.92	0.28	5	1.2	0.95	0.02	0.03	—	—	—
Ni60 (%)	0.8	4.0	—	16.0	—	—	—	—	≤ 15.0	3.2	Bal

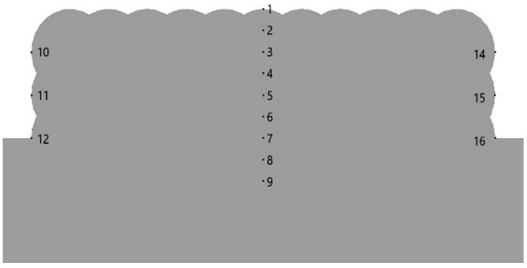

Fig. 8. Sample point location and number.

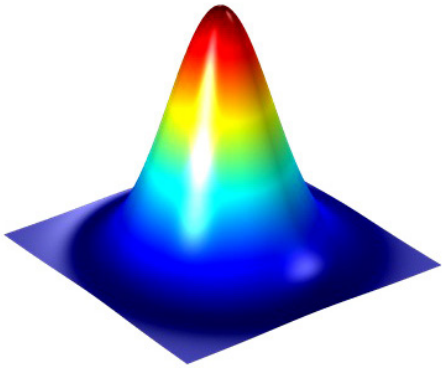

Fig. 9. Gaussian heat source 3D model.

2.3 COMSOL solution

Multi-layer and multi-pass temperature field simulation in the process of laser cladding, the Gaussian heat source model is used as the laser heat source. The laser heat source is loaded on the cladding surface, and the laser defocus is adjusted by changing the heat source radius. Physics module in COMSOL as required, the "solid heat transfer" physics module for temperature field simulation and the "deformed mesh" physics module for cladding layer dynamic simulation are selected.

3. Analysis of numerical simulation results of preheating and non-preheating

3.1 Preheating and non-preheating temperature field analysis

In the multi-layer and multi-pass laser cladding process [10, 11], the height of the cladding layer on the surface of the substrate continues to increase with the progress of the laser cladding. As shown in Fig. 10, the preheating and non-preheating laser cladding processes are used, respectively. Using the surface temperature of the substrate as the color scale, the cloud map of the surface temperature distribution of the cladding layer at three different times is rendered. At various times the unevenness of the substrate surface caused by the lap marks can be observed. At 30 s, the lowest temperature of the non-preheating surface is 799 K, and the lowest temperature of preheating is 1150 K in the first layer of cladding surface (Figs. 10(a) and (b)). At 94 s, the second layer of cladding is nearly halfway, and the lowest temperature of non-preheating and preheating on the surface of the cladding layer is 1050 K and 1320 K, respectively (Figs. 10(c) and (d)). At 158 s, on the cladding surface of the third layer, the minimum non-preheating and preheating temperatures are 1060 K and 1320 K, respectively (Figs. 10(e) and (f)). The preheating temperature is slightly higher than the non-preheating, the heat input causes the temperature of the substrate continues to increase. As the temperature of the substrate increases, more metal powders can be clad per unit time under the same laser intensity, and the cladding efficiency also increases.

Meanwhile, the difference of temperature from the first layer to the third layer is gradually shrinking, and the temperature difference in the first, second and third layers is 351 K, 270 K and 260 K, respectively. This caused by the previous layer of the cladding layer plays a certain preheating effect on the latter layer in the process of multi-layer and multi-pass laser cladding. After such thermal superposition, the temperature difference gradually decreased.

1-9 different sampling points in the middle of the multi-layer and multi-pass the cladding layer are used to obtain the temperature-time change curve in order to intuitively understand the law of temperature change of the cladding layer. As shown in Fig. 11, at 0-59 s, 64-123 s, 123-187 s are the first, second and third layer cladding stages, respectively. During the cladding of each layer, the temperature of each sampling point is increasing. At the beginning of cladding, the temperature and the efficiency of the substrate are lower. With the temperature of the substrate increasing, the cladding efficiency increased. The temperature of the sample point near the surface of the heat source has changed drastically, and the temperature of the sampling point away from the surface of the heat source has changed smoothly. Meanwhile, it can be seen that the inclination angle of the curve of the first layer after preheating is smaller than that of non-preheating, which indicates that the temperature difference between the cladding layer and the substrate after preheating is significantly reduced. Fig. 11(a) shows that the temperature of the second layer is slightly higher than that of the first and third layers. Because in the process of cladding the second layer, the first layer has a preheating effect on the second layer, and when the third layer is cladding, it has a heating effect on the second layer. Although

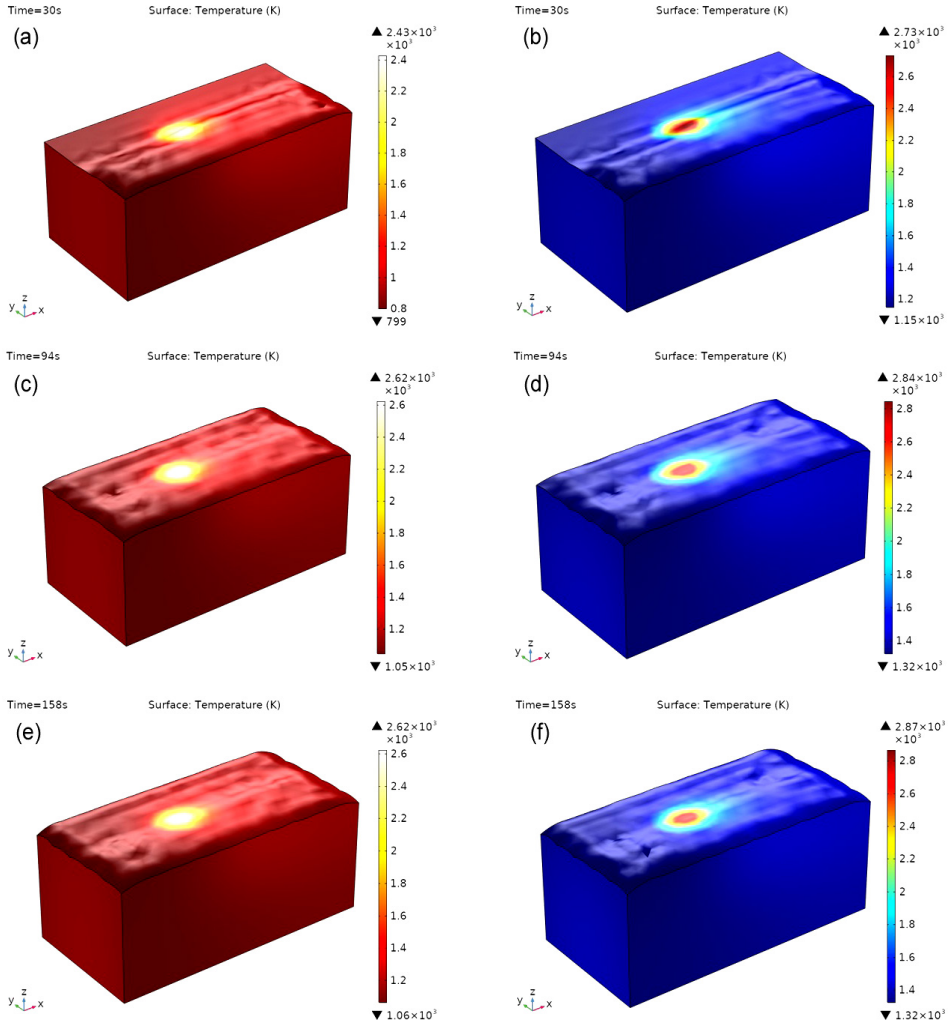

Fig. 10. Comparison of sample morphology and surface temperature field distribution at several different moments during non-preheating and preheating cladding processes: (a) 30 s without preheating; (b) preheating 30 s; (c) unpreheated 94 S; (d) 94 s; (e) non-preheated 158 s; (f) preheated 158 s.

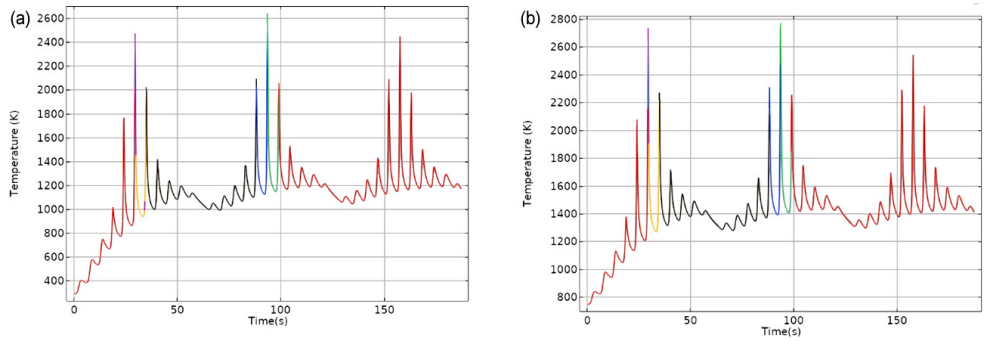

Fig. 11. Variation curves of non-preheating and preheating temperature with time: (a) non-preheating; (b) preheating.

the second layer has a certain preheating effect on the third layer, the area of the third layer in contact with the air is relatively large, and the heat dissipation is relatively fast, so the temperature of the third layer is slightly lower. In Fig. 11(b), this phenomenon is alleviated due to the preheating of the substrate in advance.

3.2 Preheating and non-preheating temperature gradient analysis

3.2.1 Non-preheating temperature gradient

With a continuous temperature field, the temperature gradient [11, 12] is a physical quantity that describes the most rapid

changes of temperature in a given regional environment in any direction and rate, which is represented by Gra. In the rapid solidification theory, the temperature gradient on the surface of the cladding layer mainly explores the formation of microstructure and macroscopic cracks [13]. The middle sampling points 2 and 7 of the first and third cladding layers are selected to compare and analyze their temperature gradients, as shown in Fig. 12.

As can be seen in Fig. 12(b), the temperature gradient values in all directions at the sampling points 2 and 7 of the cladding layer are very high. In the X, Y, and Z directions, due to the change of the position of the laser, the temperature gradient values of the sampling points at different times are different. If the temperature gradient value is positive, the temperature in the liquid phase at the front of the solid-liquid interface of the molten pool is increased as the distance from the interface is increasing, but the degree of subcooling decreases as the distance from the interface increases. If the temperature gradient is negative, it indicates that the temperature in the liquid phase at the front of the solid-liquid interface of the molten pool is decreased as the distance from the interface is increasing, and the degree of subcooling increased with the distance from the interface increasing. Compared the temperature gradient values of sample point 7 with 2 in the X, Y, and Z directions, it shows that the temperature gradient composite value of sample point 7 is significantly higher than sample point 2. Therefore, it indicates the cracks are generated at the junction of the cladding layer and the substrate. For the first and third cladding layers, the temperature gradient in the Z direction is the largest. It indicates that the crack sensitivity in the Z direction is extremely higher [14, 15].

3.2.2 Warm-up temperature gradient

As shown in Figs. 12(a) and 13(a), when other conditions are fixed, the temperature gradient value at this point decreases with the increase of the number of cladding layers, that is, the temperature gradient value at a certain point in the cladding layer is inversely proportional to the number of cladding layers. Compared with the non-preheating Z-direction temperature gradient, with the increase of the number of cladding layers, the temperature gradient value gradually decreases. As the temperature

Table 2. Experimental parameters of laser cladding.

	Laser power/W	Scanning speed/(mm/s)	Powder feeding amount/(g/min)	Track spacing/mm	Preheat laser power/W
Preheat	1500	4	15	1	500
Non-preheat	1500	4	15	1	—

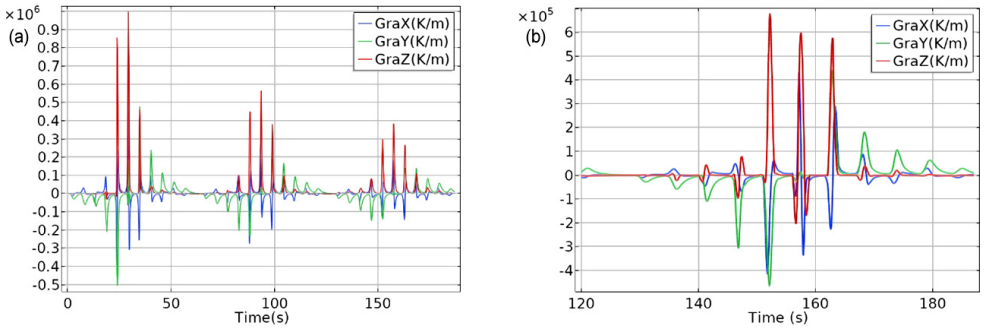

Fig. 12. (a) Temperature gradient in each direction at sampling point 7 of the first cladding layer; (b) temperature gradient in each direction at sampling point 2 of the third cladding layer. Blue: X direction; Green: Y direction; Red: the Z direction.

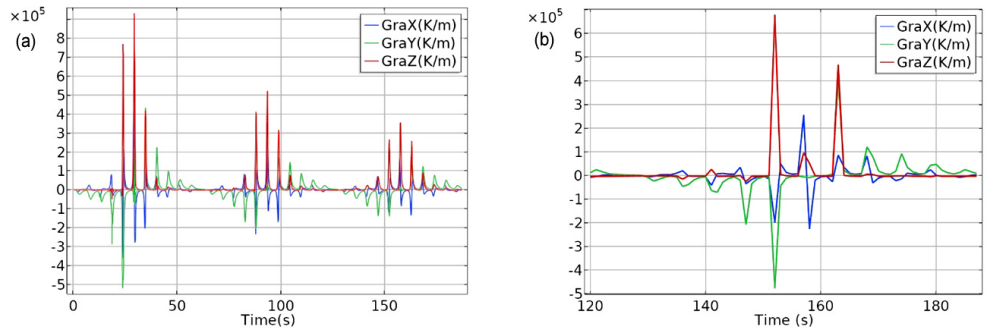

Fig. 13. (a) Temperature gradient in each direction at sampling point 7 of the first cladding layer; (b) temperature gradient in each direction at sampling point 2 of the third cladding layer. Blue: X direction; Green: Y direction; Red: the Z direction.

gradient is smaller, the sensitivity of cracks is lower. Therefore, the in-situ preheating method can effectively reduce the susceptibility to crack in the multi-layer and multi-pass cladding layer.

4. Experimental verification

4.1 Experimental materials and methods

The YLK-3000 fiber laser integrated processing system is used in the experiment. The power of the IPG fiber laser is 0-3 kw, and the powder feeding rate of the dual-channel synchronous powder feeder is 8-20 g/min. First, two substrates with a size of 40 mm × 40 mm × 8 mm are prepared. The first non-preheated substrate is coated with three layers from its surface upwards. The second substrate is preheated three times by the in-situ preheating method, and then three layers are cladded like the first substrate. The process parameters used for the two substrates are the same as those in the simulation. The experimental parameters are shown in Table 2. After the experiment is being completed, the specimen is cut along the section of the cladding layer by wire cutting. After grinding, inlaying and polishing, the cladding depth and height of the section of the cladding layer are measured under a metallographic microscope. SEM is used to observe the microstructure morphology of the cladding layer section, as shown in Fig. 14.

4.2 Preheating and non-preheating experimental morphology

As shown in Fig. 14, the simulated cladding morphology is basically the same as the results of the experiments. But the surface morphology of non-preheating has scum, and the surface morphology after preheating is smooth. After measurements, the average depth and height of the cladding layer are as shown in Fig. 14(a): 0.23 mm and 2 mm, and Fig. 14(b): 0.3 mm and 2 mm. The average height of the cladding layer obtained by the finite element model simulation is about 1.8-2 mm, and the average depth of the molten pool is 0.2-0.5 mm. It can be seen that the actual size of the cladding layer is basically consistent with the simulation results.

Because laser cladding is a process of rapid heating and cooling, the temperature gradient between the cladding layer and the matrix is very large. In addition, due to the difference of thermal expansion coefficient and elastic modulus between substrate and additive material, the cladding layer is prone to produce large thermal residual stress. The thermal residual

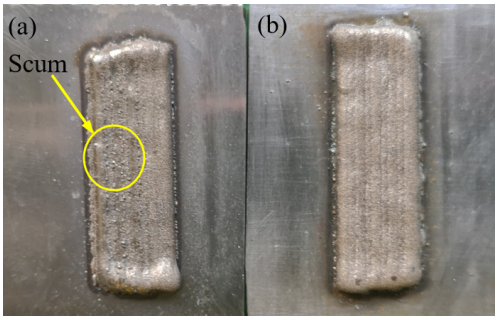

Fig. 14. Comparison of macroscopic morphology between non-preheated and preheated experiments: (a) non-preheating; (b) preheating.

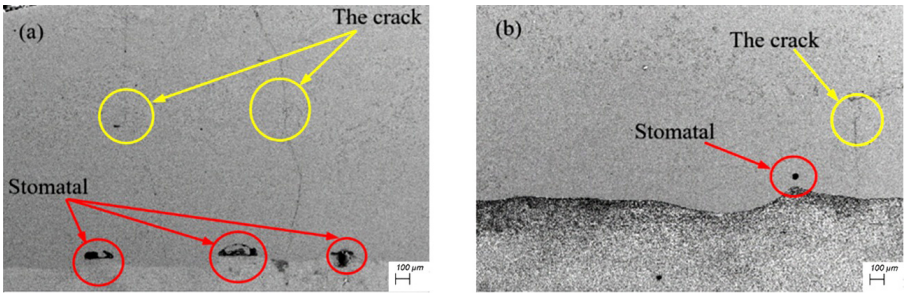

Fig. 15. SEM contrast of cross section morphology of unpreheated and preheated multilayer multipass coatings: (a) non-preheating; (b) preheating.

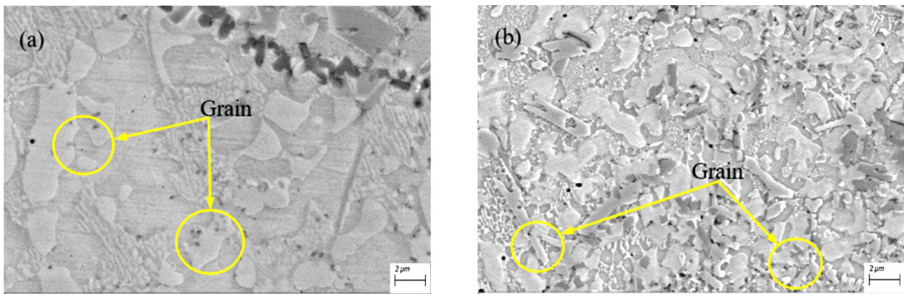

Fig. 16. Morphology of unpreheated and preheated multilayer and multichannel structures: (a) morphology of non-preheated microstructure; (b) preheated microstructure morphology.

stress is proportional to the temperature gradient and the thermal expansion coefficient is the inherent property of the material. Fig. 15(a) shows that the cracks in the cross-section cladding layer extend perpendicularly to the bonding surface of the cladding layer and the substrate to the top of the cladding layer. At the same time, the cracks and pores of the preheated cladding layer are reduced and smaller, as shown in Fig. 15(b).

This verifies the consistency of the simulation results obtained in Secs. 3.2.1 and 3.2.2 above with the experimental conclusions.

To observe the changes of the cladding layer structure more clearly, the microstructure of the cladding layer is observed with a high-power scanning electron microscope. As shown in Fig. 16, the grain structure of the non-preheating cladding layer is sparsely distributed, and the structure after preheating is denser and evenly distributed because the heat distribution of the cladding layer after preheating is uniform. Meanwhile, the grain refinement reduced the segregation of components and the damage to the continuity of the matrix, thus improving the tensile strength. Therefore, grain refinement is of great help to strengthen the cladding layer.

5. Conclusions

1) After preheating, the temperature is higher than that of non-preheating, and the cladding efficiency increases accordingly. Meanwhile, as the temperature is superimposed layer by layer, the temperature difference between the two gradually decreases with the increase in the number of layers. The temperature of the non-preheated middle layer is slightly higher than that of the bottom layer, a phenomenon which is improved after preheating.

2) The magnitude of the temperature gradient is inversely proportional to the number of cladding layers, and the temperature gradient value in the Z direction is higher than the values in the X and Y directions, which indicates that the crack sensitivity in the Z direction is extremely high.

3) After preheating, the temperature gradient value in the Z direction is significantly reduced, which shows that in-situ preheating can effectively reduce the sensitivity of cracks in the cladding layer. Meanwhile, the grain structure of the cladding layer is refined and the distribution is more uniform.

4) Using the simulated parameters to conduct experiments, the obtained cladding layer cross-section is basically consistent with the simulation results, which proves the correctness of the simulation conclusions.

Acknowledgments

This article does not have any project or personal funding, and there is no conflict of interest. The research data is transparent and can be published publicly.

References

[1] N. S. Trinity, P. S. Lesley and O. E. Olatunde, Isothermal oxidation performance of laser cladding assisted with preheat (LCAP) tribaloy T-800 composite coatings deposited on EN8, *Coatings*, 11 (7) (2021) 843.

[2] S. B. Li, J. X. Fang, S. Y. Dong, Y. J. Wang, H. S. Huang, Y. L. Jiang and B. Liu, Effects of phase transition temperature and preheating on residual stress in multi-pass and multi-layer laser metal deposition, *Journal of Alloys and Compounds*, 792 (2019) 928-937.

[3] S. Morville et al., 2D longitudinal modeling of heat transfer and fluid flow during multilayered direct laser metal deposition process, *Journal of Laser Applications*, 24 (3) (2012) 032008-1-032008-9.

[4] H. Y. Li et al., Numerical simulation of temperature field of laser cladding Stellite6 alloy on H13 steel surface, *Applied Laser*, 40 (4) (2020) 571-578.

[5] Y. Sun et al., Numerical simulation of temperature field of laser cladding multilayer coating, *Electric Welding Machine*, 51 (5) (2021) 61-65+117-118.

[6] J. G. Sun, The temperature field of simultaneous powder feeding laser multi-channel cladding and the influence of substrate preheating temperature, *Thermal Processing Technology*, 45 (10) (2016) 194-196.

[7] G. B. Liang et al., Numerical simulation study on path selection of TC4 titanium alloy laser cladding, *Journal of Henan University of Science and Technology (Natural Science Edition)*, 42 (6) (2021) 12-18+5.

[8] K. D. Patra, M. Gopinath and N. A. Kumar, High-temperature abrasive wear characteristics of H13 steel modified by laser remelting and cladded with Stellite 6 and Stellite 6/30 % WC, *Surface and Coatings Technology*, 422 (2021) 127498.

[9] C. G. Ding et al., Effects of substrate preheating temperatures on the microstructure, properties, and residual stress of 12CrNi2 prepared by laser cladding deposition technique, *Materials (Basel, Switzerland)*, 11 (12) (2018) 2401.

[10] R. S. Long and W. J. Liu, Numerical simulation of multi-track and multi-layer temperature field on laser direct metal shaping, *Journal of Wuhan University of Technology* (S3) (2006) 1111-1116.

[11] M. D. Wang et al., Numerical simulation on temperature field in multi-layers inside-beam powder feeding when laser cladding, *Key Engineering Materials*, 499 (2012) 114-119.

[12] J. Zhang et al., Numerical simulation of the temperature field in multi-layer powder-feeding laser cladding forming, *Applied Mechanics and Materials*, 184-185 (2012) 1418-1423.

[13] F. X. Fu et al., Analysis on the physical mechanism of laser cladding crack and its influence factors, *Optik - International Journal for Light and Electron Optics*, 127 (1) (2016) 200-202.

[14] G. Yang et al., Numerical simulation temperature field of laser cladding titanium alloy, *Applied Mechanics and Materials*, 117-119 (2011) 1633-1637.

[15] J. L. Song, Y. T. Li and Q. L. Deng, Optimization of laser cladding forming parameters by numerical simulation to minimize the cracking posibilitys, *Advanced Materials Research*, 143-144 (2011) 806-812.

Honggang Yin was born in Fushun, Liaoning, China, in 1995. He was a postgraduate student in the Department of Mechanical Engineering and Automation, Liaoning University of Technology. His main research interests are laser cladding, precision and special machining technology.